

A Richardson-Lucy Algorithm Using a Varying Point Spread Function Along the Iterations

Gevaldo L. de Almeida

*Instituto de Engenharia Nuclear / Reator Argonauta
Comissao Nacional de Energia Nuclear
Rio de Janeiro, 21941-972, Brazil*

gevaldo@ien.gov.br

Maria Ines Silvani

*Instituto de Engenharia Nuclear / Reator Argonauta
Comissao Nacional de Energia Nuclear
Rio de Janeiro, 21941-972, Brazil*

msouza@ien.gov.br

Erica S. Souza

*Instituto de Engenharia Nuclear / Reator Argonauta
Comissao Nacional de Energia Nuclear
Rio de Janeiro, 21941-972, Brazil*

ericasilvani@yahoo.com.br

Ricardo T. Lopes

*Universidade Federal do Rio de Janeiro, COPPE, Centro de Tecnologia
Cidade Universitaria Bloco G, Ilha do Fundao, 21945-970 Rio de Janeiro - RJ, Brazil*

ricardo@lin.ufrj.br

Abstract

Image restorations with the Richardson-Lucy algorithm suffer the usual drawback imposed by the constraint of a constant *Point Spread Function* – *PSF* as unfolding function. Indeed, even when the image exhibits a constant spatial resolution over its whole surface, an important aspect is that as the iterations advance, the overall resolution is improved while the *PSF* remains constant. This work proposes an algorithm which restores images by the Richardson–Lucy (RL) algorithm, using however, a varying *PSF* as the iterations proceed. For this purpose, the *PSF* width is reduced to cope with the last-achieved image resolution and the next iteration would be carried out with it. The process is repeated until the *PSF* does not change significantly. A main point in this procedure is *how* to evaluate the *PSF* tied to the image resolution. In this work this is performed on the grounds that the *global contrast* increases with the resolution improvement, for many gray pixels migrate towards darker or brighter regions. Hence, deconvolving an image with a steadily increasing *PSF* width, somewhere a maximum *global contrast* would be reached, corresponding to the *best PSF*. Synthetic, as well as experimental images deconvolved with the proposed technique, outperform the final quality of the same ones treated with the original Richardson-Lucy algorithm for *any* number of iterations. The algorithm and ancillary procedures have been embedded into an ad hoc written Fortran 90 program capable to generate synthetic images and process them and the *real* ones.

Keywords: Image Restoration, Deconvolution, Richardson-Lucy, Varying *PSF*.

1. INTRODUCTION

Techniques to overcome poor image resolutions may be split into two categories: efforts to produce the best possible image directly *from the oven* or/and a post-treatment. Both categories demand hard conceiving efforts, but the last one is by far more numerable, for it can be performed with a proper software, rather than sophisticated equipment. As for the second category, the ultimate goal is to restore the primordial image – that which would be obtained in the absence of degrading agents – through a post-acquisition treatment. In spite of the inherent difficulties tied to this *inverse problem* – or perhaps just because that – a plethora of methods

have been developed, improved and employed to treat images. These methods could be roughly classified into two branches: those ones requiring the previous knowledge of the Point Spread Function – PSF and those named *Blind Deconvolution* [1], [2], where both PSF and final image are simultaneously retrieved. It is well known, however, that this procedure lacks robustness and may eventually return the *same* entered image and a *zero-width* PSF [3]. Among the methods requiring a known PSF, the Richardson–Lucy [4], [5], henceforth called RL in this work, is a very popular algorithm thanks to its robustness, granted convergence to the most likely image, regardless of the image employed as initial guess, and a low-sensitivity to uncertainties in the PSF.

The RL algorithm works with a *constant* PSF along all iterations for *any* region of the image. However, an image could exhibit different *spatial resolutions* at different regions due to the features of the equipment used to acquire it. In this work, spatial resolution and PSF or PSF width are interchangeable terms, for all of them refer to the same *Full width at Half Maximum* (FWHM), – henceforth also called *width* or *w* in this work – of a bell-shaped distribution. This distribution may emerge as the response of an imaging system to a point-like source, and in this case, it is referred to the PSF of the system.

Since there is a defined relationship between the lens focal distance and the gaps of the object and its image to the lens, there is only a certain range – depth of field – where the image is acceptably sharp. This means that the PSF should be rather *depth-variant*, but unlike the SPIM fluorescence microscopy [6] it is not possible to *illuminate* a selected plane. An alternative technique replaces this illumination by cropping the PSF directly from the image itself, provided that it contains small and isolated enough structures [7].

An image may also exhibit a *spatially-variant* PSF – as some astronomical ones – a phenomenon caused by the optical aberration of the telescopes, for which some methods [8], [9] have been developed to deal with.

Hence, in order to apply a constant PSF one should choose a PSF-width which yields the best overall image quality.

A hybrid method [10], using *blind deconvolution* and the RL algorithm has been as well developed, applying a PSF, iteratively determined, but employed solely to recover *synthetic single-plane* images of small sizes. Another work [11] determined the PSF by smoothing several of them, obtained through the known technique of differentiating the *edge response functions* (ERF). However, one of the main points addressed in the present work – namely the dealing with a *variable spatial resolution* over the image pattern – was not addressed, for the ERFs were acquired for a single plane. More recently, an evaluation of the PSF width based upon *edge detection and fuzzy logics* [12] has been proposed for restoration of the images of satellites. It however demands spatially invariant, and weakly or moderately degraded images.

Hence a *best* PSF – which would yield the best overall image quality – should be somehow employed. However, even *if* the *best* PSF were known, there is still another constraint: along the deconvolution, the image is continuously being improved but the unfolding PSF is kept *constant* as required by the RL algorithm, i.e., the image is deconvolved with a *shifted* PSF width.

This mismatch is *eliminated* in this work by reducing the PSF width as the iterations proceed in order to cope with the resolution of the last deconvolved image. Such a procedure requires the knowledge of the resolution of the image so far achieved. This is performed with an algorithm based upon the concept of *Global Contrast* (*G-value* for short) [13] as addressed in section 2.

For the same number of iterations, the proposed algorithm demands a greater computational effort. Yet, the higher quality of the final restored image outperforms by far that obtained with the conventional RL approach for any number of iterations, making thus worthwhile the additional computational effort. Furthermore, the lower number of iterations required to reach the steady-

state precludes an excessive noise amplification, a shortcoming which led to the development of damped versions of the RL algorithm [14], [15] to mitigate this phenomenon. Another *plague infesting* the RL algorithm is the *artifact* appearing due to the discontinuity at the image boundaries, as illustrated in the section 3.1, which led to the development of techniques to mitigate it, such as [16].

2. METHODOLOGY

The proposed methodology is not tied to any type of acquisition system, as it uses solely the information provided by the image itself. Synthetic images have been also generated with an ad hoc written program to evaluate the soundness, capabilities and limitations of the methodology. This approach allows a free choice of relevant parameters otherwise unfeasible or too expensive to achieve.

2.1 Deconvolution with a Varying PSF Along the Iterations

The flow diagram sketched in Figure 1 highlights the differences between the conventional RL procedure and the proposed one.

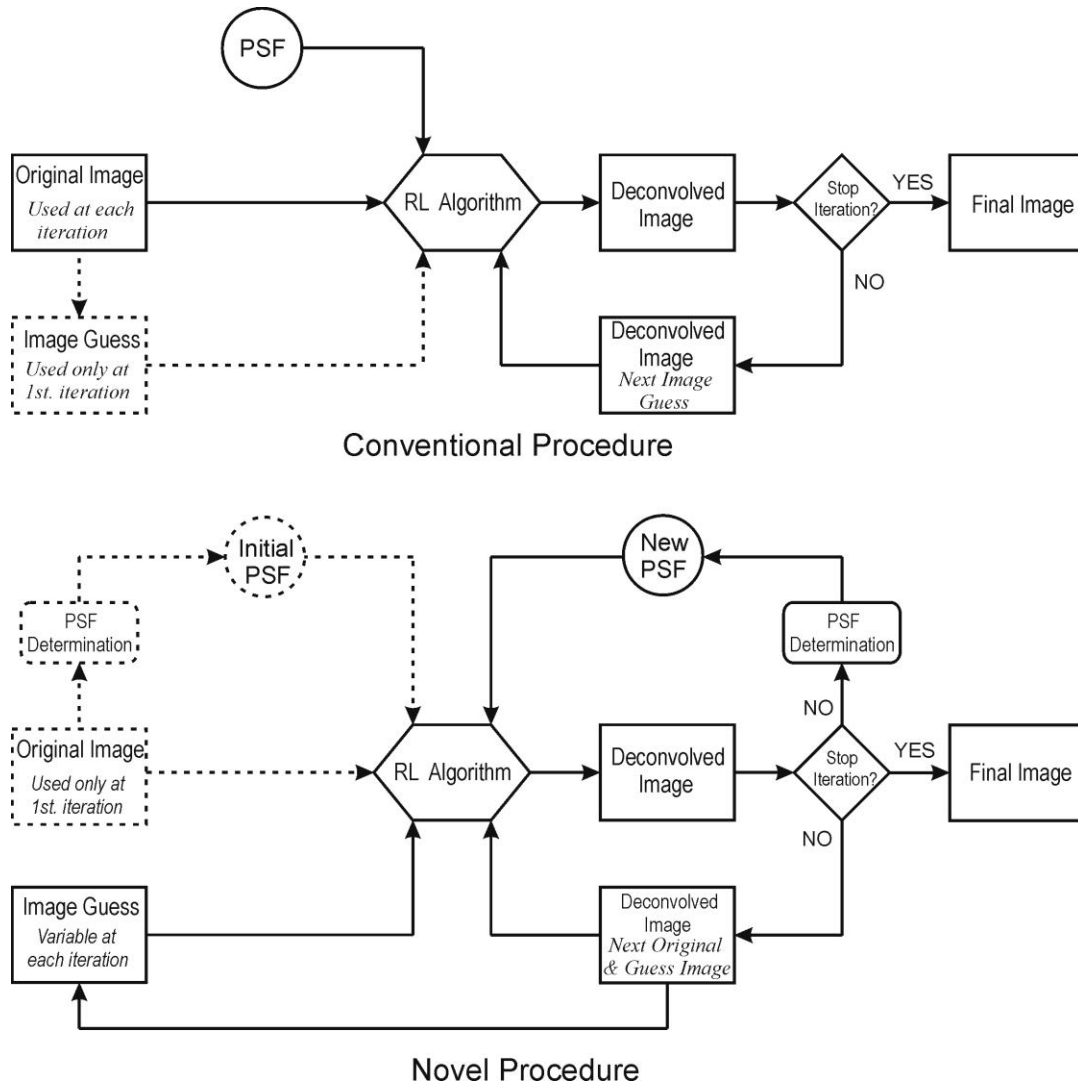


FIGURE 1: Conventional and novel procedures to restore images by the Richardson-Lucy algorithm. Dashed lines represent actions performed only at the 1st iteration. Unlike the original procedure, the novel one uses a varying PSF which is determined prior to each iteration.

In the first one, the Original Image, a specified *constant* PSF, and an initial Image Guess are delivered to the RL algorithm, which using always the original image and the last deconvolved one performs a sequence of iterations with the *same* PSF until a certain condition is reached. Unlike the PSF and the Original Image which are used for all iterations, the Image Guess is used only once – a feature represented by dashed lines – and can be the original image itself, as used in this work, or *any one* of the same size and same pixel/mm.

In the novel procedure, the iterations are carried out in a similar way, except that the New PSF arising from the last deconvolved image is used to deconvolve the next one. Its assessment – PSF Determination – is performed through the concept of *Global Contrast* as addressed in section 2.1.1. The Original Image is used only once, for – as the Image Guess – it is replaced by the last deconvolved one.

2.1.1 Determination of the Best PSF

An essential requirement to vary the PSF along the iterations is to determine its value after the last iteration in order to apply it in the next one. A PSF is fully characterized by its shape and width w , but it is assumed in this work that it has a Gaussian distribution. An image, however, may exhibit different resolutions over its surface obliging thus the researcher to choose an *effective* one, i.e., that yielding the best overall image quality. For that, one would have to scan a broad range of PSF widths, and for each of them to carry out about 20-30 iterations. The final images (one for each PSF width) should then be compared.

A visual inspection, besides its subjectiveness, would be a hard, boring and cumbersome task to make the comparison. Instead, this work employs an algorithm which transduces the *Global Contrast* [13] into a *single number*. This is done by searching for the PSF width w yielding the *best* image (highest G-value) after 3 iterations performed with the conventional RL approach. It is still necessary to scan a broad range of PSF widths but only 3 iterations (instead of 20-30) for each of them. After an initial PSF width w , a chosen increment is added to w and a new set of 3 iterations is carried out. Further details can be found elsewhere [13].

The G-value increases with w , reaches a maximum, and then decreases again. Solely 3 iterations are sufficient to reach an acceptable steady value, making this approach an affordable technique. The w -value yielding this maximum is assigned as the *best* PSF width and used for the image deconvolution by the conventional RL algorithm. For the varying PSF algorithm, the same approach is applied, but the *best* PSF width is determined after the 3 iterations carried out for each entered w . The G-value is determined as follows:

$$G = \left[\sum_{i=1}^M \sum_{j=1}^N u(i, j) \cdot \beta(i, j) \right] \left[\sum_{i=1}^M \sum_{j=1}^N u(i, j) \cdot |1 - \beta(i, j)| \right]^{-1} \quad (1)$$

$$\beta(i, j) = 0 \quad \text{for} \quad u(i, j) \leq u_m \quad (2)$$

$$\beta(i, j) = 1 \quad \text{for} \quad u(i, j) > u_m \quad (3)$$

$$u_m = (M \cdot N)^{-1} \cdot \sum_{i=1}^M \sum_{j=1}^N u(i, j) \quad (4)$$

where:

$u(i, j)$ = Pixel value at the point (i, j) .

M, N = No. of columns and lines of the image matrix.

As stated by equation (4), u_m is the average pixel-value of the whole image, which is used to classify all pixels into two classes: below and above it. The sums of all pixel-values occurring above and below u_m constitute the numerator and denominator of equation (1) respectively, defining the G-value, while the bump function $\beta(i, j)$ defined by equation (2) and equation (3) classifies the pixel-values as below and above u_m respectively.

This formalism is justified as follows: after a deconvolution with a given PSF width w , many pixels in the gray region shift towards darker or brighter regions due to the penumbra reduction. Hence, the histogram tails raise with a consequent lowering of the remaining profile, for its area must be conserved.

A higher fraction of pixels at darker and brighter zones means a higher contrast arising from a better resolution. Therefore, the sum of all pixel-values above u_m would increase while that below it would decrease, resulting into a higher G-value. This is illustrated with the histogram in Figure 2 arising from raw and deconvolved gamma-ray radiographic images of an old-fashioned film-camera. Further details can be found elsewhere [13]. Yet, for the sake of completeness, additional information concerning the determination of the *best* PSF-width, including some data from [13] are addressed in the next paragraphs.

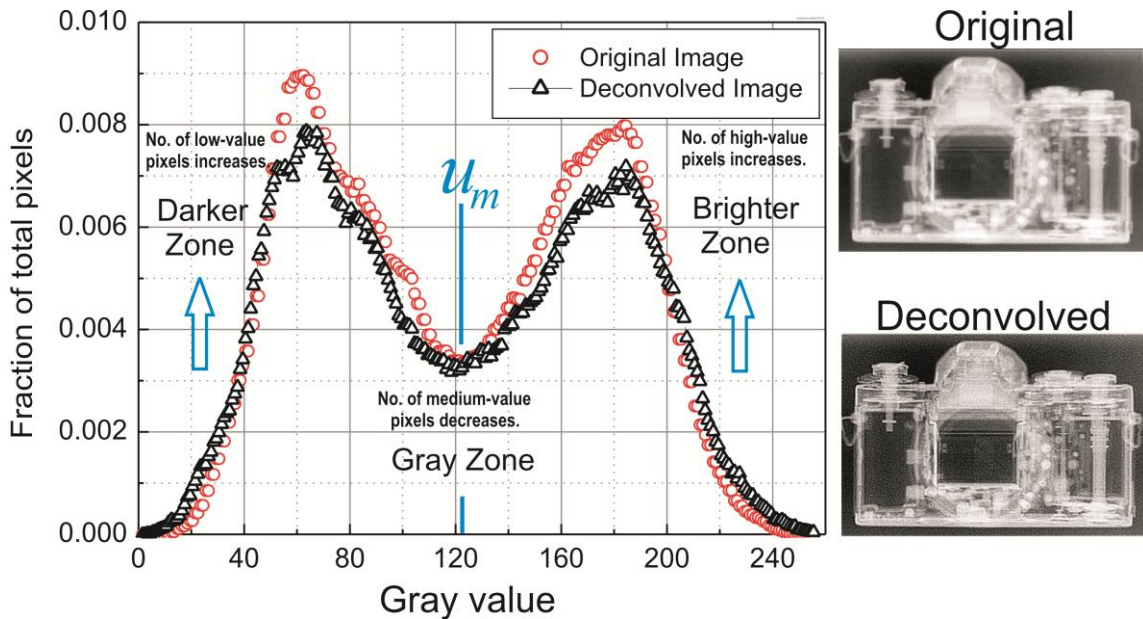


FIGURE 2: Actual histograms of a raw and a deconvolved image produced by gamma-ray radiography [13]. The resolution improvement shifts some pixels from gray zones toward brighter and darker ones raising the tails and lowering the middle zone.

As observed in Figure 3, reproduced from [13], 3 iterations carried out with the conventional Richardson-Lucy algorithm with a constant PSF-width are sufficient to achieve an acceptable convergence. Both graphs have been obtained as follows.

An initial PSF-width is used as a *Deconvolution* w . After a certain number of iterations, varying from 1 to 5, the *global contrast* is computed for the input image. Next, an increment is added to that initial w and a new *global contrast* is determined. It initially increases with w , reaches a maximum and then decreases. The abscissa of this maximum defines the *best* w for the deconvolution with the Richardson-Lucy algorithm.

It can be noticed that for the synthetic image (left), the convergence to the *best* w occurs already at the 1st iteration for each input w . The experimental image (right) – a thermal neutron

radiograph of an aeronautical turbine stator blade – requires however 3 iterations (for each input w , as well). This difference is most likely caused by the different object thicknesses. Indeed, while the synthetic image emulates the neutron radiograph of a flat object, the experimental one arises from a thicker device, which casts a broader range of spatial resolutions.

The best PSF-width yields always the best overall image quality, for a given number of iterations. If this number increases, that quality becomes improved, but the best PSF-width remains the same. Indeed, the Fig. 3 shows an increasing global contrast with the number of iterations but the peak epicenter keeps its position. Hence, 3 iterations used to determine the best w , constitute simply a representative sample. Should this number be replaced by a larger one, no different result would arise, but the CPU time would be enlarged with no advantage at all.

The *best w* determined for the original image, may be then employed as a constant PSF-width by the deconvolution with the conventional Richardson-Lucy algorithm. For the same procedure using a varying PSF-width, as here proposed, this parameter must be determined prior to each deconvolution.

Therefore, an image restoration performed with a varying PSF involving n deconvolutions, would require $3.s.n$ operations, where s is the number of PSF widths used to scan a given domain encompassing the *best w*. The best w for the original image lies in the domain between zero and a certain *unknown* maximum, which should be conservatively set as a large value. For the subsequent images, that maximum is assigned as the *best w* obtained for the previous image, making thus possible to define a domain. A further processing can be then automatically performed by the program as addressed in section 2.4.

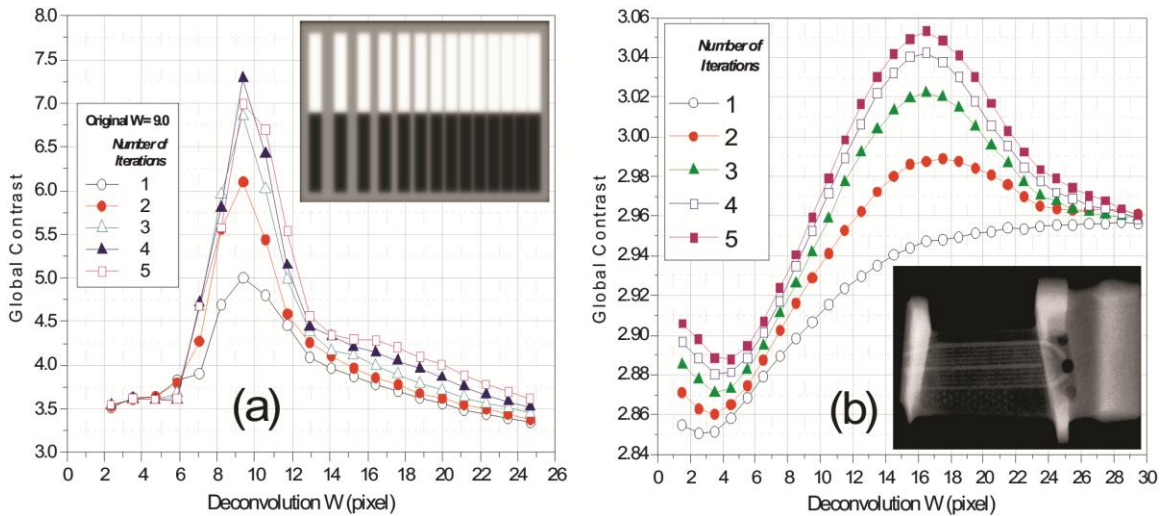


FIGURE 3: Convergence to the best PSF-width w , as posited by the Global Contrast approach. A thermal neutron radiograph of a turbine stator blade (right) requires a larger number of iterations than the synthetic image (left), most likely due to the broader range of spatial resolutions [13].

2.2 Synthetic Images

Although not developed in this work, the *global contrast* algorithm deserves a special analysis due to its paramount importance in the proposed Richardson-Lucy algorithm using a varying PSF. This analysis encompasses the algorithm response to several image patterns, e.g., different spatial resolutions and contrasts, as expected to occur in general imaging. To achieve this task, synthetic images are generated, making it possible to produce a customized image pattern.

This section therefore addresses 3 main purposes:

- a) Generate images with a wide range of contrasts and spatial resolutions.

- b) Verify the soundness of the *global contrast* algorithm through its response to a wide range of contrast and spatial resolutions as addressed in section 2.2.1.
- c) Apply the proposed *Richardson-Lucy with a varying PSF* algorithm to the synthetic images to verify the consistency of the obtained results (Section 3.1).

Once the topics a) and b) are properly addressed and shown their soundnesses, then, it is possible to rely on the results arising at topic c).

Optical images may exhibit regions with different spatial resolutions and contrasts. In this work, they are produced by an ad hoc program simulating a geometrical arrangement comprised by a test-object, a surface light source and a screen where the image is projected. The maximal achieved brightness is normalized to a pixel intensity of 65,535.

The test-object is constituted by 25 thin square blades of different transparencies, attached to a fully transparent support, as sketched in Figure 4.

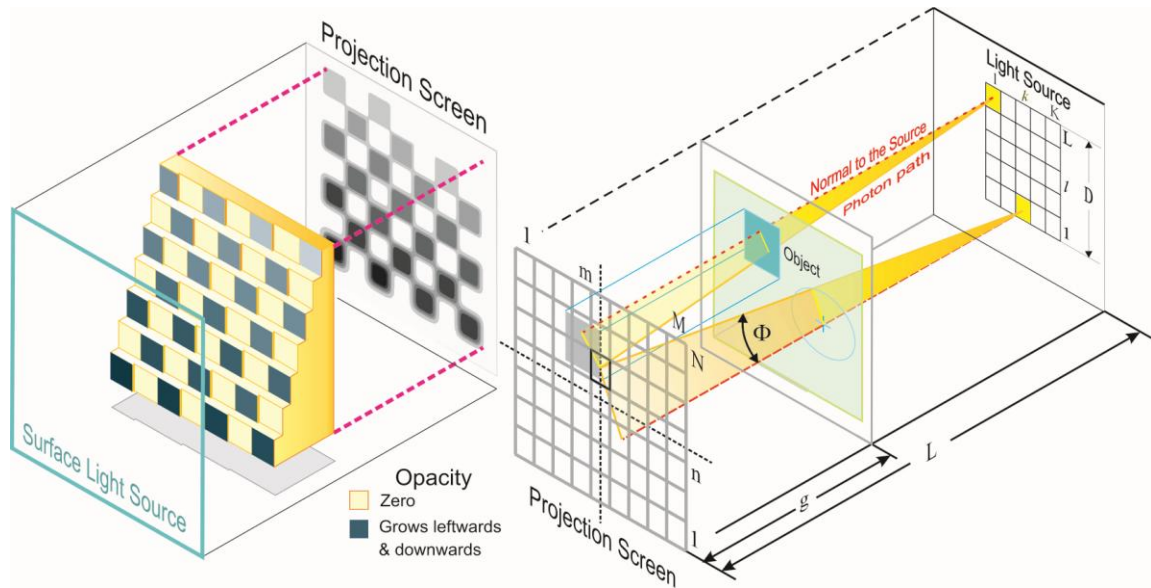


FIGURE 4: Test-object (left) and the arrangement to generate the image (right). Each pixel on the projection screen – one is highlighted – is hit by the photons from the source and eventually attenuated by a blade. Their contributions are ruled by the parameters L , D , g and by the blade opacity.

They cast individual shadows of different brightnesses and blurs, depending upon their transparencies and gaps to the projection screen respectively. The parameters L , D and g rule the spatial resolution of the generated images. A resolution of 0.05 mm/pixel has been assigned to the image projected on the screen.

The algorithm to generate the synthetic images deals solely with 3D analytical geometry and the Lambert's law of attenuation. A projection screen receives the photons coming from a $D \times D$ square source of light at a distance L , after passing through the object. For simplicity, only one attenuating blade contained in the plane at a gap g from the projection screen is represented. It can be realized that the L/D ratio rules the maximal angle Φ between a photon path $z(k,l,m,n)$ and the normal to the source element where it comes from.

It is assumed that the photons are isotropically emitted by the source elements, and do not undergo any dispersion or reflection but solely attenuation as they traversed the square blades. The highlighted pixel on the projection screen is within a penumbra region because it receives all photons coming from the highlighted source element at the bottom, but only part of them –

depending upon the attenuation factor of the intercepting square blade – coming from its upper companion. This penumbra region grows with D/L and g .

To obtain the intensity map of the image cast on the screen of $M \times N$ pixels, a light source of $K \times L$ square elements is placed at a distance L from the screen. Each pixel value $p(m,n)$ depends upon the angle $\Phi(k,l,m,n)$ defined by the coordinates on the screen and on the light source as expressed by equation (5).

This value depends upon the source intensity, its distance to the screen and the attenuation of the i^{th} square blade. All these parameters are condensed into a single value normalized to the 65,535 limit of a tiff-image.

$$p(m,n) = \sum_{k=1}^K \exp[-f_i \cdot \Omega(k,l,m,n)] \sum_{l=1}^L I_0 \cdot [L/z(k,l,m,n)] \quad (5)$$

where:

$p(m,n)$ = Pixel value on the detector: $m=1$ to M , $n=1$ to N .

f_i = Light attenuation factor of the blade i . $i=1$ to 25.

$\Omega(k,l,m,n)$ Bump function: 1 if the photon hits the blade i , 0 otherwise.

$z(k,l,m,n)$ = Length of the straight line connecting the pixel (m,n) on the screen with the (k,l) element on the light source.

I_0 = Reference intensity.

L = Distance source-screen.

K = No. of elements along the source width.

L = No. of elements along the source height.

M = No. of pixels along the image width on the screen.

N = No. of pixels along the image height on the screen.

The *bump function* value is assessed through the interception of the straight line $z(k,l,m,n)$ with the blade i . The *reference intensity* I_0 encloses the source intensity. Any number can be chosen for I_0 since the matrix $p(m,n)$ will be normalized to the maximum tiff-value of 65,535. The last term $L/z(k,l,m,n)$ is a geometric correction to cope with the photons arriving at the screen in a non-perpendicular fashion. The $M \times N$ matrix is then stored for further processing and plotting by the same Fortran program embedding the described algorithm.

2.2.1 Response of the Global Contrast Algorithm to Different Image Configurations

The deconvolution with a varying PSF requires its determination prior to each iteration. Due to the paramount importance of this determination to the proposed RL algorithm, some typical cases are addressed. Images may exhibit a huge number of different patterns, precluding thus a comprehensive evaluation of the algorithm capability and robustness to deal with all of them. Yet, it is possible to analyze its response to some specific cases by *manufacturing* virtual test-objects at customer's design. As this task requires solely 3D analytical geometry and program writing, it is a matter of trade-off how far one should go. Within this frame, some typical test-object configurations are addressed in the next sections, each of them yielding a different image pattern. All of them are comprised of 25 attenuating blades after a chess pattern, distributed along several gaps to the screen. The images cast by them on the screen have been inverted for the sake of a better visualization.

2.2.1.1 Response to an Image Cast by a Single Plane Object

An object comprised of a single plane parallel to the screen – as that described in section 2.2, but compressed to a *zero* thickness – represents an instance with a *variable* contrast and a *constant* spatial resolution. It simulates the conventional photo of a chess-pattern flat square where the single elements exhibit different brightnesses. Since their gaps to the camera are the same, their

blurs in the image would as well be identical. The resulting degraded image, its deconvolved companion (50 iterations, $w=4.2$ pixels) and its undegraded version (the flat object attached directly to the screen) are shown in Figure 5. The best PSF to restore the degraded image with the conventional RL algorithm has been determined by the G-value approach, yielding a width of 4.2 pixels as shown in the same figure. The test-object size has been limited to 34x34 mm to spare processing time.

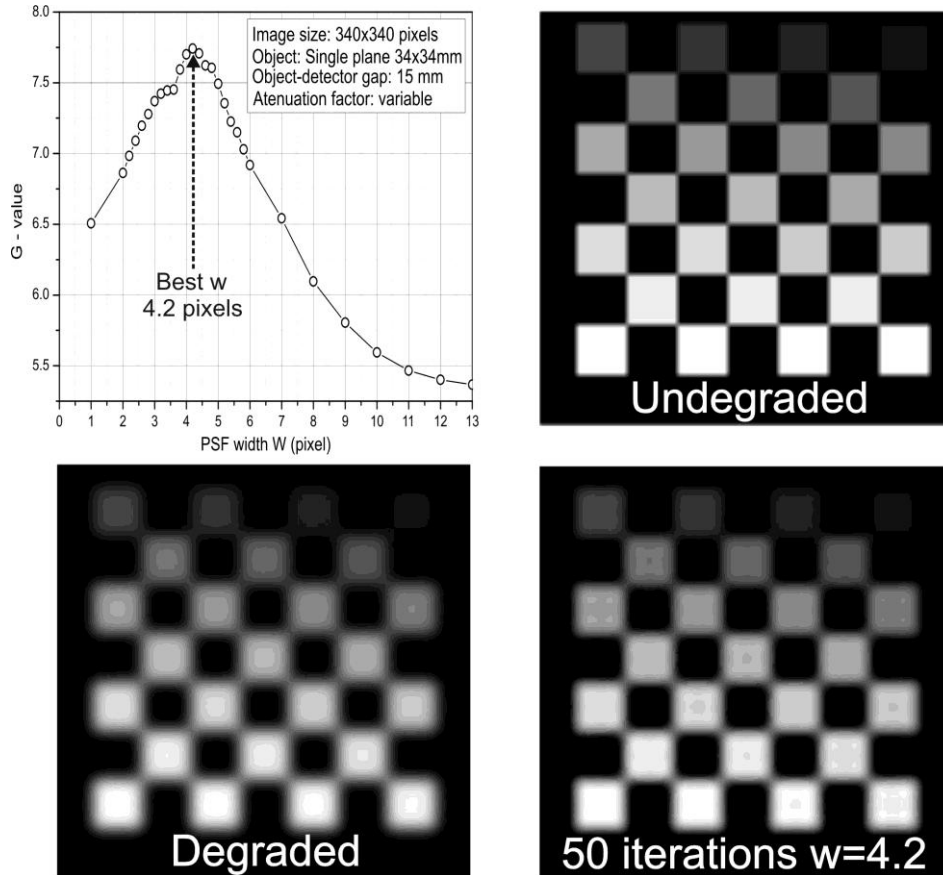


FIGURE 5: Degraded image and its restoration by the original RL algorithm. The attenuating blades were at 15-mm gap to the screen. The best PSF width for the deconvolution was furnished by the graph. An undegraded image is also shown for reference.

2.2.1.2 Response to Images Cast by Multi-plane Objects at Reversed Configurations

This section analyzes the impact of the brightness of the square blades and their gaps to the screen upon the determination of the *best w*. It would be equivalent in a conventional photo, as if the bright subjects were farther from the camera than the darker ones, and another photo were taken with the inverse configuration. To perform this simulation, a rotation of the object at 180° around its vertical axis, would invert the gaps of the high and low-attenuating square blades to the screen. Each blade contributes with its own gap to the *best w*, but the brighter the shadow it casts on the screen, the greater its contribution. Therefore, low-attenuating blades – exhibiting a corresponding low-contrast – become so faint when placed at large gaps that can be overwhelmed by the prevailing background. Under such a condition, the high-attenuating blades, closer to the screen, drift the *best w* towards their own positions.

Mutatis mutandis, the high-attenuating blades despite their larger gaps still exert a great influence thanks to their high brightnesses. Indeed, as shown in Figure 6, when the high-attenuating blades (casting bright shadows, for the images have been inverted) are located at large gaps, the corresponding curve L exhibits a maximum G value at $w=4.5$ pixels. In the inverse configuration –

curve S – the G value reaches its maximum at $w=1.8$ pixels, i.e., the overall image quality should be better. This forecasting is corroborated by the attached images.

It can be noticed that the G values themselves reach different amplitudes. This happens because the image generated by blades at large gaps is more luminous than its companion as inferred from the attached images. Indeed, for high-attenuating blades at short gaps, the low-attenuating ones would be located at large gaps, and thus, could not contribute significantly to the overall image luminosity due to the overwhelming prevailing background.

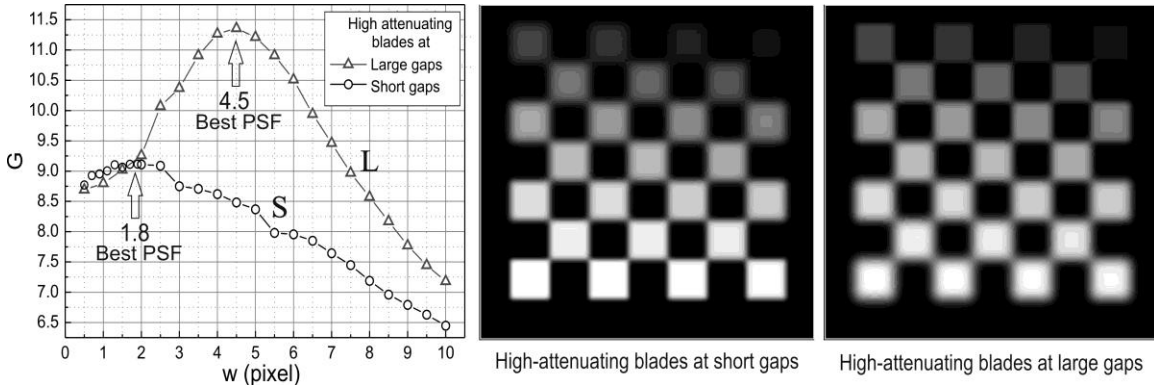


FIGURE 6: High-attenuating blades at short gaps (curve S), displaces the best w to a value (1.8 pixels) tied to the average of their positions, while the images of the farther low-attenuating blades become so faint that are overwhelmed by the background. In the reversed configuration, the high-attenuating blades still exert its influence thanks to the high brightness of their cast images which shift the best PSF to $w=4.5$ pixels.

2.2.1.3 Response to Images Cast by Multi-plane Objects of Different Thicknesses

This section addresses the response of the *Global Contrast* algorithm to images exhibiting the same *contrast* range as in previous section, but different *spatial resolution* ranges. To generate them, 5 test-objects of several thicknesses – containing also 25 square blades under a chess pattern – have been employed. A minimum gap from the closest square blade to the screen has been kept at 5 mm for all objects, while the farthest one has been placed at 10, 15, 25, 35 and 45 mm. The intermediate blades have been regularly distributed between these limits.

To analyze the impact of these different image patterns upon the *best w*, the *global contrast* algorithm has been applied. As shown in Figure 7, a larger range of the blade-screen gap yields a larger *best w*. As expected, farther blades to the screen cast on it images with poorer resolutions, and thus, a larger w .

Five different normalized profiles ($G \times PSF$ width w) are shown, one for each test-objects thickness: 5, 10, 20, 30 and 40 mm, encompassing the blade–screen gap ranges 5-10, 5-15, 5-25, 5-35 and 5-45 mm respectively. The profile broadening with the object thickness should somewhat be expected, since the individual PSF widths w , related to each blade shadow are more spread out. At any rate, these results match with those obtained in previous sections.

One can observe that the profile for the 5-10 mm gap at the left of the graph, unlike its smooth companion 5-45 mm, exhibits a strong ripple. It most likely comes from arithmetic truncation and roundness, since the written Fortran program deals with discrete pixel intensities. Yet, as this drawback occurs at low PSF widths, it would affect only the last iterations, where a steady state should already be reached.

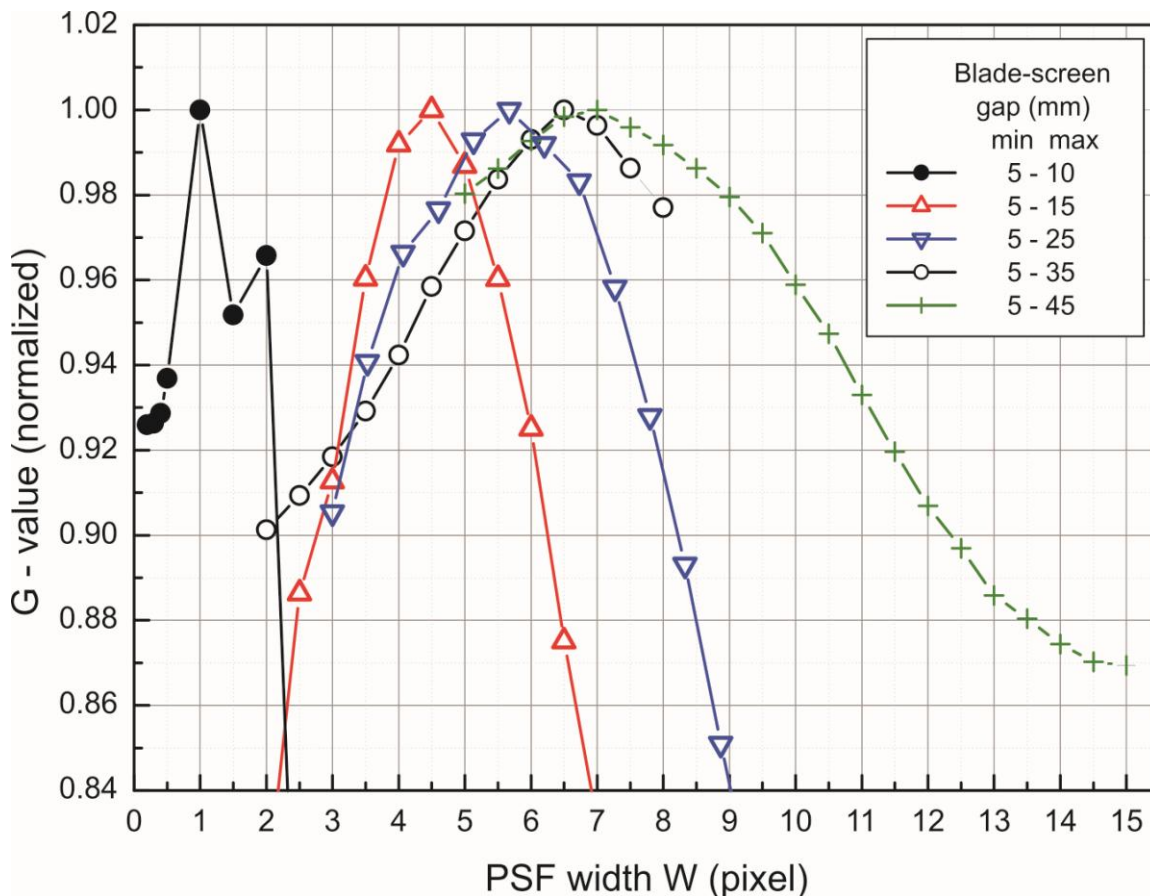


FIGURE 7: Response of the algorithm to 5 different gaps ranging from 5-10 to 5-45 mm. The closest insert is always 5 mm apart from the screen, while the others are equally distributed until the maximum gap. As expected, large gaps increase the *best w*.

As inferred from the analysis performed along this section 2.2.1, different image configurations – of resolution and contrast – yield different PSF widths and should be accordingly deconvolved, after the concept of *best PSF*. Hence, even if the conventional RL algorithm applies this PSF at the 1st iteration, it is unquestionable that the resulting deconvolved image is improved. Therefore, the PSF that should be applied to deconvolve this new image should have a *narrower* width w , in order to match with the new achieved resolution. Nevertheless, the soundness of this concept must be verified through deconvolution of synthetic and experimental images with the conventional RL algorithm, as well as with its modified version employing a varying PSF as here proposed. This topic will be addressed in section 3.

2.3 Experimentally Acquired Images

The technique to restore images by the RL algorithm with a *varying* PSF is proposed on the grounds that the image undergoing deconvolution is being improved along the iterations. Hence, each image obtained after a given iteration has its own overall resolution and should be accordingly deconvolved, i.e., with a certain *best PSF* width w , which yields the best quality after each iteration.

Once this value is obtained for the original image – as determined by the *global contrast* algorithm – it can be used as the unfolding *constant* PSF width in the usual RL algorithm or applied to the modified one. At any rate, the values of w do not depend upon the equipment or means employed to acquire the image, but solely on the information contained in its pattern.

Within this frame, besides the synthetic images, two experimentally acquired neutron and gamma-ray radiographic images have been selected as examples, due to their wide range of contrasts and resolutions. Details of their acquisition are superfluous and beyond the scope of this work.

2.4 Automatic Deconvolution with a Varying PSF Along the Iterations

As the *best w* is defined by the maximum *G-value*, the process is automatized avoiding thus a cumbersome task to the researcher. After the technique employed in this work, the PSF-width domain is scanned with a chosen subinterval in order to detect the maximum *G-value*. The abscissa of this maximum on the graph $G \times w$ defines the *best* PSF width to deconvolve the image. As shown in Figure 8, each image *i* is deconvolved with its own *best* PSF width w_i previously determined by the *global contrast* algorithm.

For this determination, the RL and the *global contrast* algorithms are applied to the image *i*. A conventional RL deconvolution with 3 iterations for each PSF width along the domain is then carried out. The resulting global contrast is plotted against the PSF width *i*, until a maximum is reached. This width is assigned as the Best PSF width, which it is input into the same image *i* together with the conventional RL algorithm which performs one *single* iteration, yielding the image *i+1*, and the procedure is repeated until the Best PSF width for the *i*th image does not change significantly.

Except for the original IMAGE 0, where a maximum PSF width could not a priori be assigned, for all the subsequent ones this maximum is obviously the PSF width of the last image. This limit reduces the domain to be scanned, saving thus CPU time. Yet, a certain tolerance is allowed to deal with expected ripples in the curve *Best PSF x Iteration Number* as will be seen in section 3.

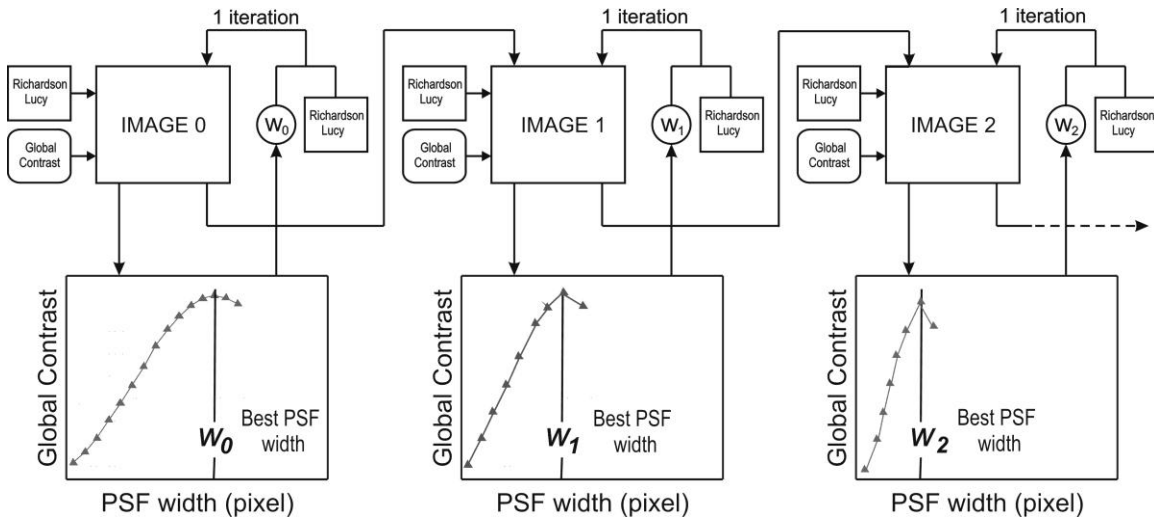


FIGURE 8: Automatic procedure to apply the Richardson-Lucy with a varying PSF along the iterations. Each iteration is carried out with the RL algorithm and a PSF width w_i previously *extracted* from the image itself with the *Global Contrast* algorithm. The iterative process is interrupted when the PSF width w_i stabilizes.

As the iterations proceed, the spatial resolution, i.e., the PSF-width (*best w*) to deconvolve the current image decreases, diminishing thus the domain encompassing it. A tolerance for the higher limit of this domain is assigned, avoiding thus an eventual impact of ripples. This limit is defined as $L_f = f \cdot w$, where *f* is a parameter greater than 1. (in this work a conservative value of 1.1 has been chosen) and *w* is the spatial resolution from the previous image.

A shorter subinterval is required to scan a narrower domain, in order to assure a proper number

of points on the graph *global contrast x PSF-width*. The program then, uses a subinterval $s=h.w$ where h is a constant parameter previously chosen by the customer.

3. RESULTS

3.1 Synthetic Images

A synthetic image, as described in section 2.2, has been used as benchmark to check the soundness of the developed algorithm. The left graph in Figure 9 depicts a family of normalized $G \times w$ curves from images deconvolved with the proposed procedure in the range 0–7 iterations. So, 4.5 pixels is the PSF width for the iteration 0, i.e., the original image.

Prior to each iteration, the *best w* is determined through the maximum G -value arising from equations (1–4). The right graph simply reproduces the related maxima versus the iteration number for the sake of a better visualization. For both algorithms (conventional or modified) subsequently deconvolved images exhibit a decreasing w . Yet, for the varying PSF option, the best PSF width drops faster demonstrating that it is more effective than the conventional one using a *constant* PSF. Indeed, the upper curve in the right graph – expressing the *best w* obtained along the iteration under this condition – exhibits higher PSF widths, except obviously for the 1st iteration. Due to the asymptotic behavior, the iterations have been interrupted at the 11th one. Both options, however, exhibit *artifacts* and a trend to shrink the squares as shown in Figure 10.

As this phenomenon is not tied to the proposed technique – but as well known, to the RL algorithm itself – it does not constitute a drawback to its implementation and application. At any rate, better images are achieved with a varying PSF. An undegraded image is also shown for reference.

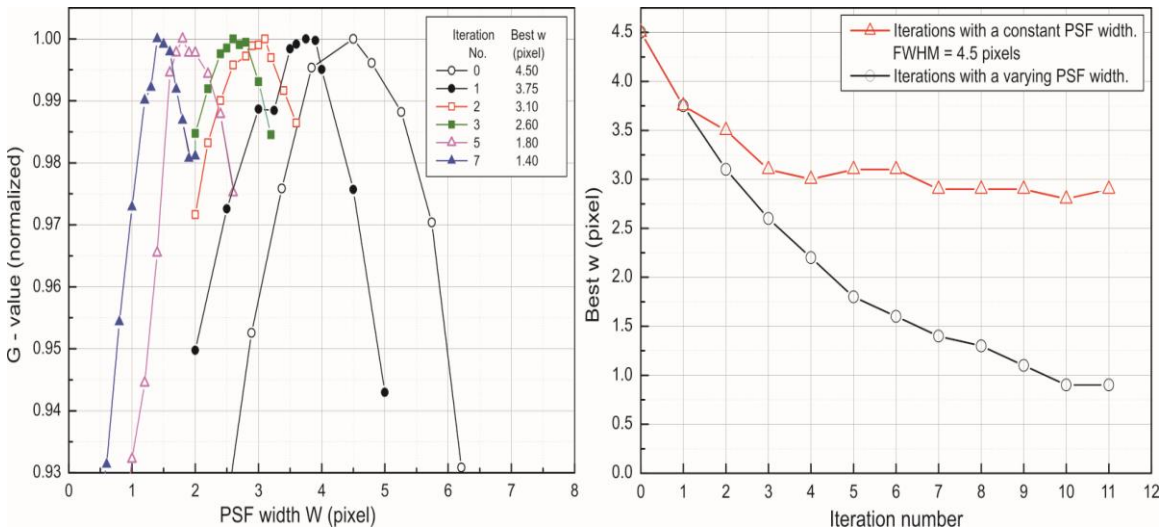


FIGURE 9: Family of curves G -value \times PSF width (left) and their related *best w* \times iteration number (right) for deconvolution with a varying PSF (lower curve). Deconvolution with a *constant* PSF (upper curve) is less efficient as the *best w* drops at a slower rate and reaches a higher value at the asymptotic region.

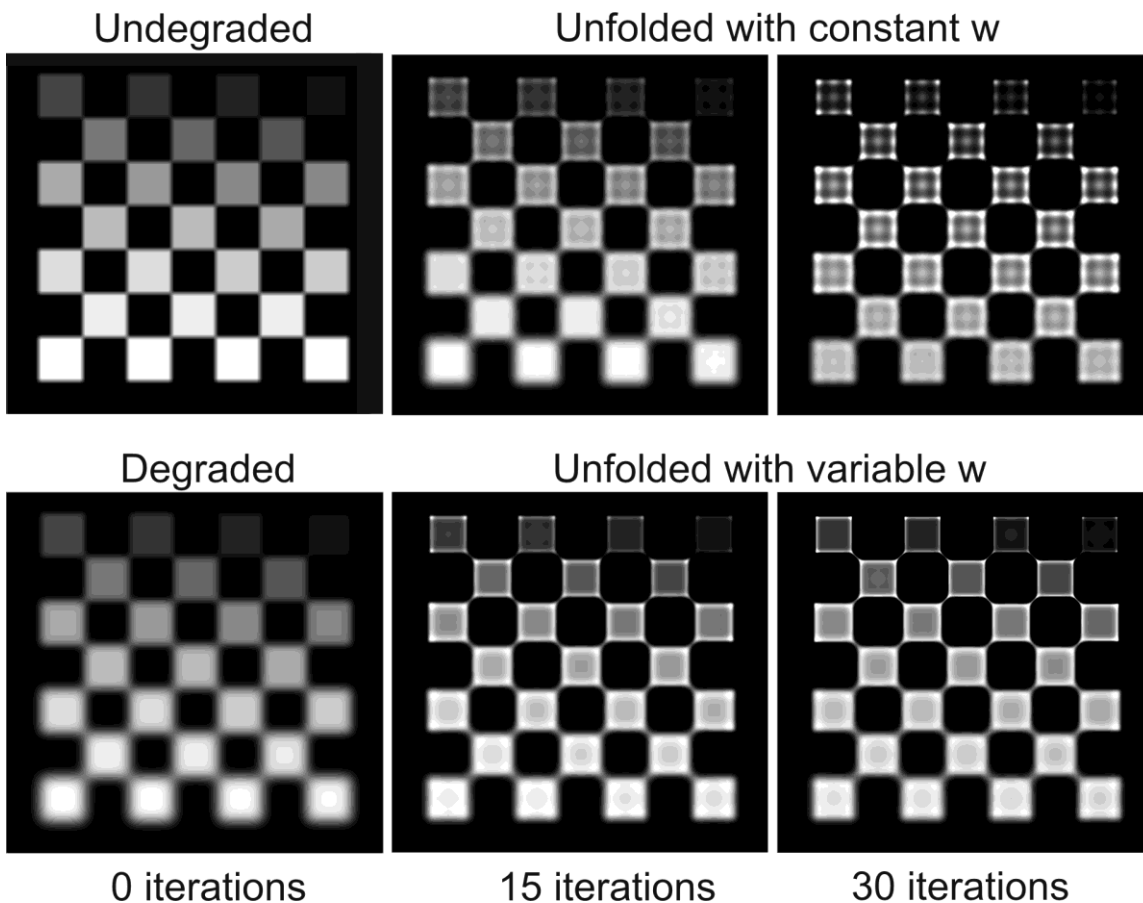


FIGURE 10: Synthetic images unfolded with *constant* and *varying* PSF widths, ratify the higher performance of the last approach. Artifacts arise with both procedures but the unfolding with a varying PSF yields a better image quality. An undegraded image is also shown for reference.

3.2 Experimental Images

Experimental neutron and gamma-ray radiographic images of an old-fashioned film-camera have been elected due their large range of contrasts and resolutions. The means, conditions and parameters for their acquisition will not be addressed, as they are irrelevant for the image treatment. Both images undergo the same treatment but are separately dealt, for the sake of organization.

3.2.1 Thermal Neutron Radiographic Image

As in the synthetic case, each image is deconvolved with its *best w* determined through the *G-value*. The related graphs and images are shown in Figure 11 and Figure 12 respectively. It can be noticed that 10 iterations carried out with a varying PSF outperform those processed with a constant value, even for 50 iterations. The first option, however, in spite of the lower number of iterations, demands a higher computational effort. Yet, as the whole process is managed in an automatic fashion by the program itself, the only drawback is the long required CPU time.

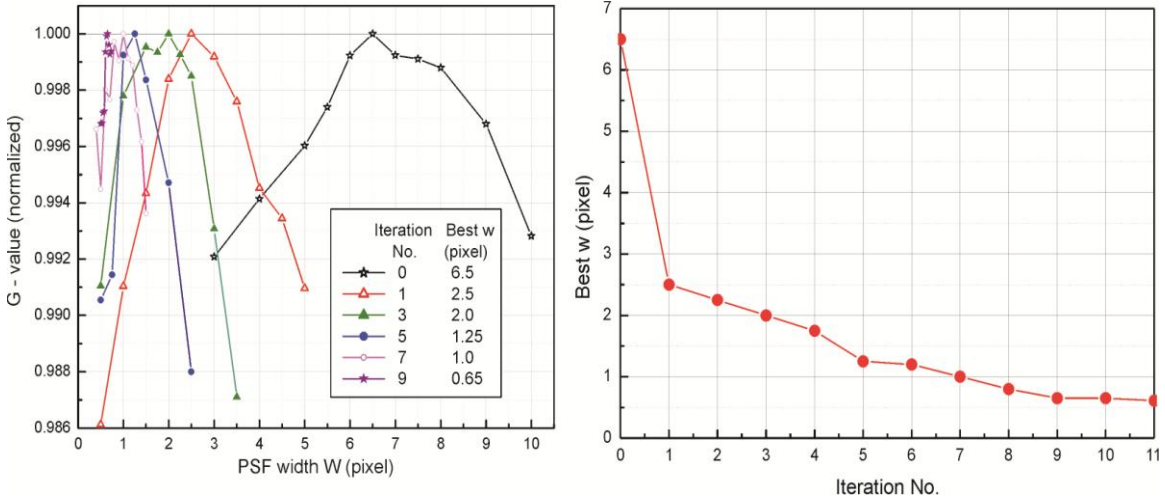


FIGURE 11: Family of curves G -value \times PSF width W (left) and the related $Best\ w \times$ Iteration No. (right). Iterations were interrupted at the 11th one, for the $best\ w$ converges to about 0.5 pixel.

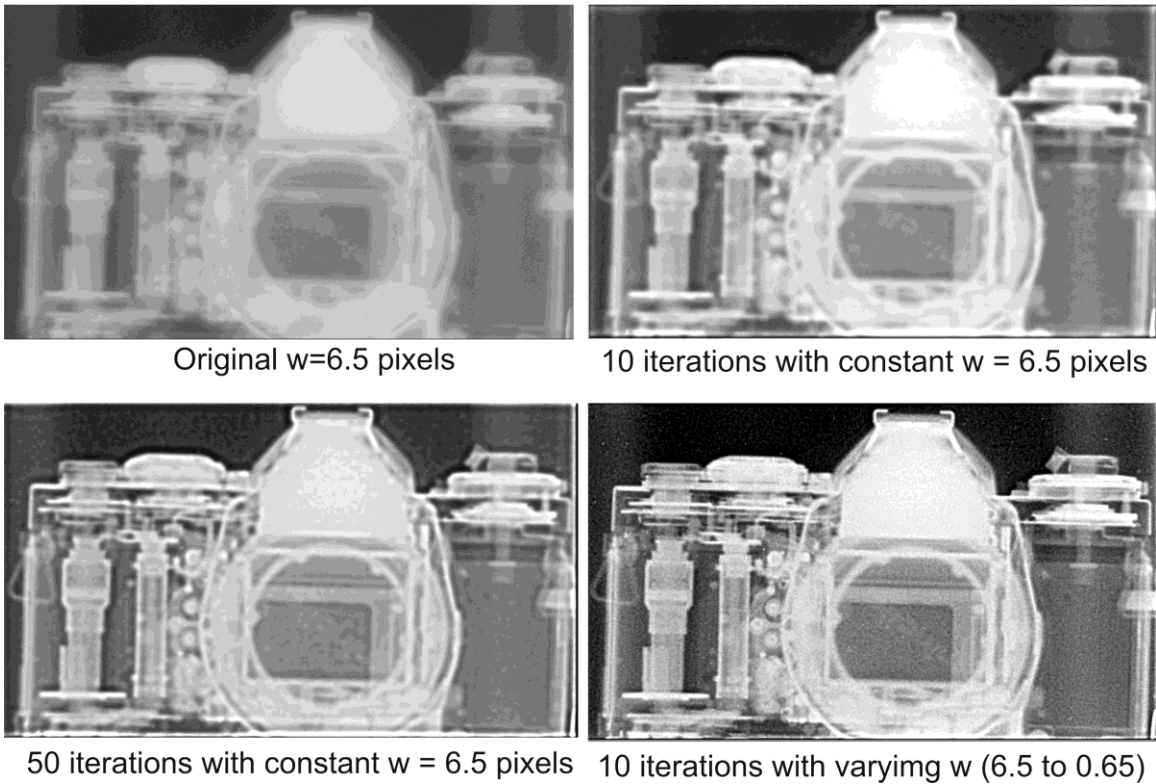


FIGURE 12: Original and deconvolved neutron radiographic images of a film-camera. 10 iterations carried out with a variable PSF outperform those done with a constant value even for 50 iterations. The first option however, despite the lower number of iterations, demands a higher computational effort.

3.2.2 Gamma-Ray Radiographic Image

The results obtained with a gamma-ray radiographic image are presented in Figure 13. It can be noticed that the original image exhibits a much better overall resolution than that achieved with neutrons, an outcome tied to nuclear physics parameters which will not be addressed here. As for the restored images, those deconvolved with a varying PSF also exhibit a better quality. Indeed, 8 iterations carried out with a varying PSF outperform 50 iterations with a constant PSF .

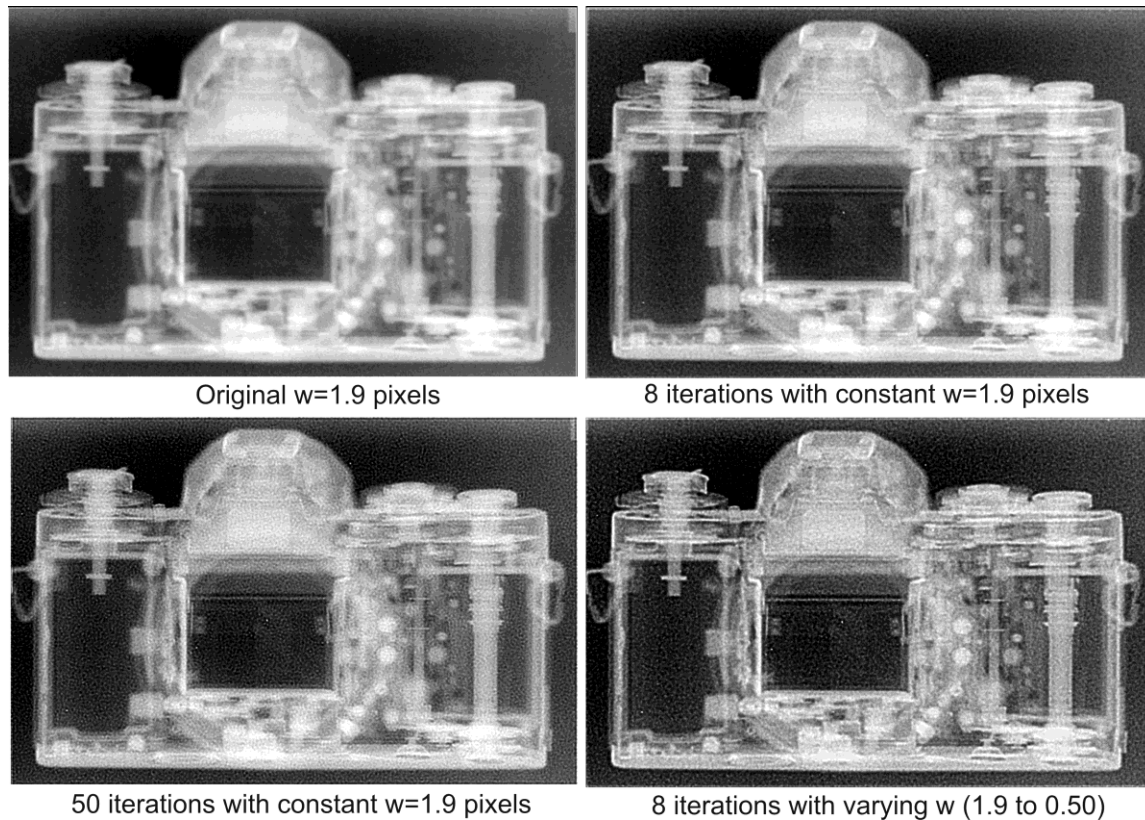


FIGURE 13: Original and deconvolved gamma-ray radiographic images of a film-camera. Eight iterations undertaken with a varying *PSF* outperform those done with a constant value, even for 50 iterations.

3.3 Cross-Check of the Varying PSF Approach

As inferred from the previously presented images and graphs, a *varying* PSF along the iterations yields better images than a *constant* one. However, due to this unique RL approach, it is highly advisable to perform an additional cross-check of the procedure.

It has been already shown that an image deconvolved with a constant PSF width – as determined by the *global contrast* algorithm – arising from the image itself, exhibits a poorer quality than that deconvolved with a varying PSF. It is therefore important to verify what would be the result, if the image were deconvolved (using a constant PSF) with the *narrower* PSF width emerged at the end of a process employing the *varying* PSF technique. An important point of this verification is to ratify that *only* a *varying* PSF along the iterations produces the best results, i.e., the *initial* or the *final* resolution (arising from the varying PSF option) *do not* produce the best image when applied to the original RL algorithm.

The impact of the PSF width of 6.5 pixels onto the neutron radiographic image deconvolved with this constant value is presented in Figure 14. When this value is used as *initial* PSF width in the varying PSF approach, after 10 iterations, the image exhibits a PSF width of 0.65 pixels, as previously shown in the graphs of Figure 11. A deconvolution by the original RL algorithm with this constant value of 0.65 pixels – i.e., the final resolution achieved at the end of the 10 iterations with a varying PSF– likewise *does not* yield the best image as shown in Figure 14, an outcome which is ratified by the graph in Figure 15. Indeed, the ratio 2.7/0.65 indicates *quantitatively* that (for this image) the proposed modified RL algorithm produced a final image about 4 times better than those ones arising from the original one.

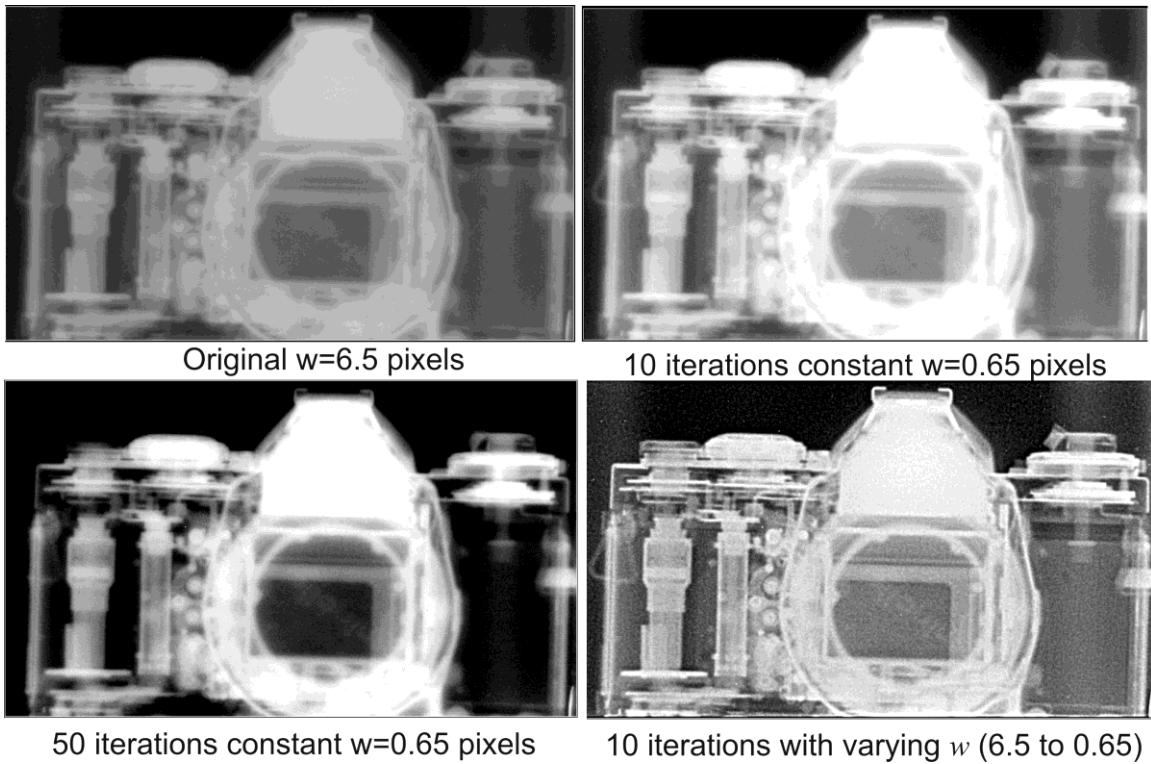


FIGURE 14: Neutron radiographic image deconvolved with a constant PSF of 0.65 pixels (the resolution achieved at the end 11 iterations with a varying PSF). The original image and that one deconvolved with a *varying* w are also shown for comparison.

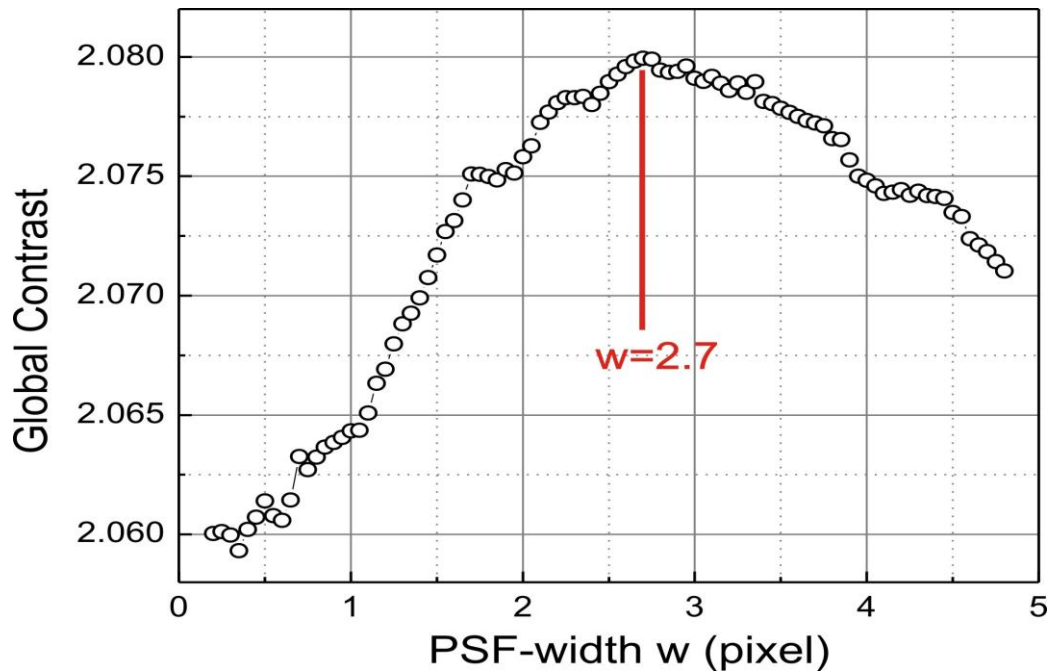


FIGURE 15: *Global Contrast* \times *PSF-width* for the neutron radiographic image deconvolved with 10 iterations under a *constant* PSF-width of 0.65 pixels, i.e., the value reached by the same radiograph deconvolved with 10 iterations under a *varying* PSF, starting with 6.5 pixels.

3.4 Comparison with Other Works

To the best of the authors knowledge, no work dealing with a RL algorithm using a varying PSF along the iterations has been yet reported in the literature. Therefore, a comparison can be done only with other *different* techniques. Among the immense number of developed techniques, *blind deconvolution* is more close related to this work, for it as well, determines the PSF, though *simultaneously* with the final deconvolved image.

The Figure 16 shows images of a spiral CT temporal bone (a), restored with the blind deconvolution approach (b), as given by [2]. The original image (a) has been as well restored in the present work with the conventional (c) and the proposed (d) RL algorithms respectively. Both images, (a) and (b), have been retrieved from the original paper as a *png* file, amplified 2x using the bilinear interpolation option of *ImageJ*, which converted it to a *jpg* format and delivers a matrix with pixel values. The *jpg*-values of this matrix have been then converted to *tiff* format, precluding thus, that the *integer* pixels values arising from the convolution of the PSF with the image matrix, could be *too early zeroed*.

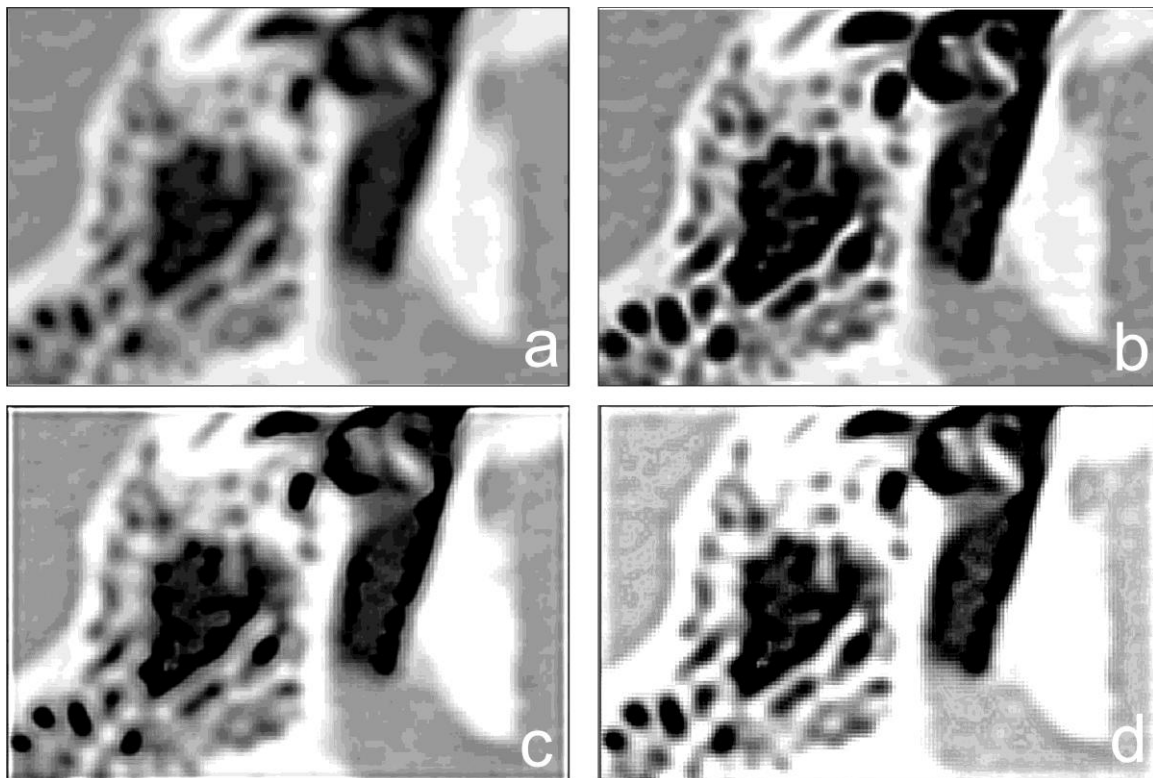


FIGURE 16: Original spiral CT image of a temporal bone (a), and its blind-deconvolved companion (b) [2]. Deconvolved images of the raw image (a) with the Richardson-Lucy algorithm under a constant PSF(c) and with a varying PSF along the iterations (d) are shown for comparison.

As expected, the image processed with a varying PSF exhibits a better quality than its companion processed with a constant one. Yet, a visual inspection shows that its quality is inferior to the blind-deconvolved image. It is therefore worthwhile to compare this visual evaluation with the quantitative outcome arising from the *global contrast* technique as follows.

After the graph *Global Contrast x w* shown in Figure 17 (left), the blind-deconvolved image (b), exhibits a spatial resolution of 0.45 pixels. This outcome from an image acquired by an *independent* researcher, corroborates once more, that the *global contrast* approach – an essential tool supporting the proposed *varying PSF* approach – behaves consistently, i.e., its *G x W* curve exhibits a *maximum*.

The curve *Best w x Iteration No.* (right), for the deconvolution of the same original image (a) under a varying PSF, exhibits its typical behavior. An included zoom of its asymptotic tail shows the *Best w* crossing the determined PSF-width for the blind-deconvolved image (0.45pixels) - represented by the horizontal line – at the 11th iteration and fairly stabilizing afterwards at circa of 0.3 pixels, an outcome that does not match with the visual evaluation. Although not possible to assert that this is caused by the compulsory *digging* and digital treatment – imposed by the unavailability of original image (a) – it is as well not possible to exclude this explanation.

Until other studies - with adequate images - could be conducted by independent researchers, it is not possible to analyze the performance of the proposed method with regard to other techniques. Nevertheless, the examples here presented demonstrated the superior performance of applying a *varying PSF* along the iterations to the R-L algorithm, but further verifications should be carried out by independent researchers.

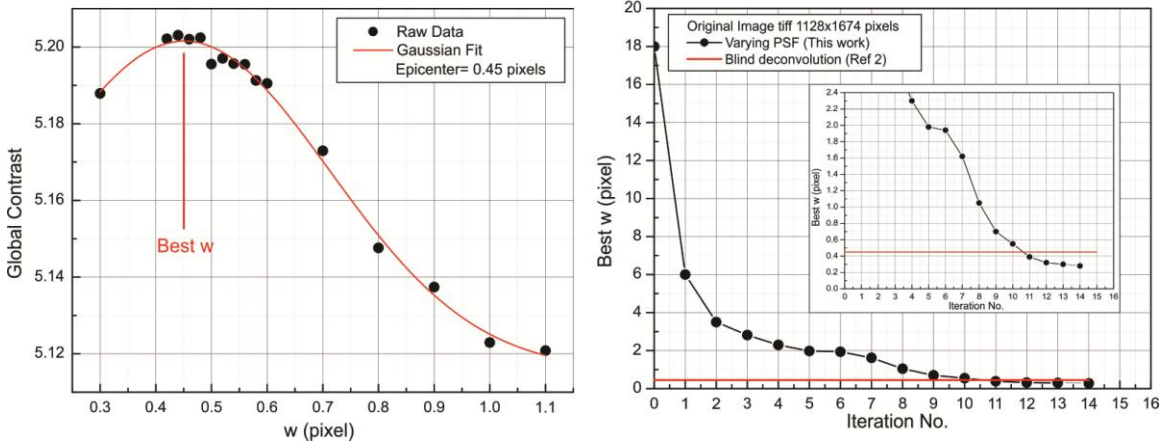


FIGURE 17: *Global Contrast x w* profile arising from the *global contrast* approach (left), for the blind-deconvolved spiral CT image of a temporal bone [2]. The same raw image deconvolved with the *varying PSF* technique yields a final *best w* at 0.28 pixels as observed at the asymptotic region of the curve *Best w x Iteration No.*(right).

Whether the abscissa of this maximum *really* represents the best *w* to unfold *any image* at all, is a matter of verification through a visual inspection with *many* different images.

Yet, as far as the images here analyzed are concerned, both the *varying PSF* along the iterations and its ancillary *global contrast* tool are sound procedures.

4. DISCUSSION

The posited technique to restore images by the RL algorithm with a varying PSF-width along the iterations, yielded consistent results, for synthetic, as well as for actual experimentally acquired images. Once verified that, besides the results obtained in Ref [13], the *global contrast* algorithm reacted consistently to several other different image configurations, a solid basis for its application could be asserted. Yet, it should be pointed out that any other approach capable to replace the visual evaluation by a single number (as done by the *global contrast* technique) would be applicable to the proposed method.

The basic idea behind the method is to unfold an image with *its own* spatial resolution or PSF-width. If two researchers receive the same images to restore, but the image delivered to one of them had been undergone a previous partial deconvolution, (with 1 or 2 iterations), they certainly would realize that their images exhibit different qualities, and would infer that they arise from systems possessing *different* resolutions.

The final image furnished by a system is the outcome of a convolution between the primordial (*unknown*) image and the PSF of the system. With a *fully characterized* PSF the image would be retrieved simply by solving a linear system of equations. Unfortunately, this ideal solution may be applied only – as a demonstration – to extreme minuscule (a couple of pixels) matrices, and thus, useless for the imagery field. Indeed, for useful images (even those of modest sizes), the huge coefficient matrices (a $n \times n$ image requires a $n^2 \times n^2$ coefficient matrix), roundness and truncation required to cope with the required *integer* pixel values for the image, generated ill-posed matrices, precluding to solve the system. This constraint led to the development of iterative techniques, as the RL algorithm.

But even with a *fully characterized* PSF, the primordial image could *never* be retrieved, due to this *ill-posed* inverse problem. Only the most likely resembling image could be achieved. Hence, if it is already a hard task to get an *approximate* image, even with an *exact* PSF, it is not an efficient and reasonable approach to *abdicate* of it in favor of a less precise value. In other words, the PSF-width employed at the 1st iteration – disregarding whether it is correct or not – should not be used in the remaining ones, since the deconvolved images are being improved, and their PSF-width concomitantly *narrowed*.

Furthermore, the *varying PSF* approach is expected to be more forgiving to uncertainties in the initial PSF with because – disregarding whether the 1st deconvolved image has been improved or additionally degraded due to an improper w – in the subsequent iterations the deviation would be corrected. This correction should occur because the *global contrast* algorithm would determine the PSF width of the 1st deconvolved image (improved or degraded), and its value employed to correctly deconvolve it.

Switching back to the example of the two researchers, in order to perform a proper deconvolution of their images with the RL algorithm, they *need* a fully characterized PSF, i.e., its shape and width (FWHM). If they use an eventual technique to evaluate the PSF, certainly they would find *different* outcomes, because the partially deconvolved image would exhibit a better quality due to the improvement performed by those previous iterations. So, if the 1st researcher keeps its evaluated PSF-width, along the whole deconvolution procedure (as prescribed by conventional the Richardson-Lucy algorithm), it would be carried out under a *shifted* PSF-width. Indeed, while the 2nd researcher started with a *narrower* value (due to the previous iterations), the 1st one would still be applying its broader PSF at the 2nd, 3rd and further iterations.

An image deconvolved with a *zero* PSF-width would not be modified at all. It would be equivalent to an acquisition performed with an *ideal* system. Under such a circumstance, the system would have not degraded the primordial image, and thus, there would be *nothing* to be corrected. Indeed, it is a well-known *blind deconvolution* drawback, that this approach sometimes delivers an *unmodified* input image together with a *zero* PSF-width. On the other hand, a PSF with a larger width than that tied to the image itself, not only would not improve it properly, but could even degrade it. Somewhere, between these limits lies the best PSF-width, reproducing the *effective* spatial resolution of the image.

As the PSF shape is very difficult to obtain, it is usually replaced by a radially symmetric 3D-function. In this work a Gaussian has been employed with fairly good results. However, it is not possible to assure that it is the best function to restore the images presented in this work (nor other images as well). It is therefore an open field for researchers working in image restoration, to seek for better unfolding functions (PSF shapes) and algorithms to replace the image pattern by a single number representing its overall quality, as done by the *global contrast* approach.

An important feature of an algorithm is naturally its *robustness*. However, it only can be assured through a *large* number of restorations with *different* images by different researchers. Such a task should be performed through many researchers, due to the *huge* number of runs involved, and to assure *independent* verifications. The impact of the proposed technique in the field of imagery

constitutes, as well, an even wider – and hard – field to explore, due to the true zoo of image restoration methods. A comprehensive comparative study would be a herculean burden.

This work aims rather a far less ambitious target, namely, to propose a procedure to vary the PSF width along the iterations in the RL algorithm, and compare the resulting images with those arising from a constant PSF.

Future research aiming at to strengthen this technique and establish its robustness, capability and limits, could include, e.g., the study of various PSF shapes and its impact on the final image quality, the search of other approaches to evaluate the PSF, the combination with other techniques in hybrid methods, such as, stopping criteria for the iterations, damping RL algorithms, elimination or reduction of artifacts, and naturally a robustness evaluation of the proposed method, through an extensive verification involving images of several spatial resolution and contrast ranges.

5. CONCLUSION

A novel procedure is proposed to restore images by the Richardson–Lucy algorithm, using however a *varying* Point Spread Function – PSF along the iterations. Within this approach, the spatial resolution of the image obtained at the last iteration is used as the PSF width (w) for the next iteration, until it does not change significantly. The w -value is assigned as that yielding the greatest *Global Contrast*, on the grounds that it increases with the image spatial resolution, for many gray pixels migrate to darker or brighter regions. Although applied in this work only to synthetic, neutron and gamma-ray radiographic images – as well as, to a spiral CT image for the sake of comparison – the procedure may in principle be applied to images of any kind, since all the required data are provided by the images themselves. The only *alien* required parameter is the PSF shape. A 3-D Gaussian function has been used in this work, but other ones could produce better results, an eventuality which deserves a more comprehensive evaluation involving different functions, and images. As the spatial resolutions of the images are essential to perform this evaluation, they should be somehow determined by using the technique employed in this work, namely the *global contrast* concept, or any other suitable one. At any rate, despite the unusual use of the Richardson-Lucy algorithm, the promising results obtained in this work deserve a deeper analysis from researchers working in the image restoration field.

6. REFERENCES

- [1] D. Kundur and D. Hatzinakos, “Blind Image deconvolution”, Signal Processing Magazine IEEE, Vol. 13, No. 3, pp. 43-64, 1996.
- [2] M. Jiang, G. Wang, “Development of Blind Image Deconvolution and its Applications”, Journal of X-Ray Science and Technology Vol.11, pp. 13-19. 2003
- [3] F. Tsumuraya, N. Miura, N. Baba, “Iterative Blind Deconvolution Method using Lucy’s Algorithm”, Astronomy and Astrophysics, Vol. 282, pp. 699-708, 1994.
- [4] W. H. Richardson, “Bayesian-based Iterative Method of Image Restoration”, Journal. of the Optical Society of America, Vol. 62, No. 1, pp. 55-59, 1972.
- [5] B. L. Lucy, “An Iterative Technique for the Rectification of Observed Distributions”, The Astronomical Journal, Vol. 79, No. 6, pp.745-754, 1974.
- [6] M. Temerinac–Ott, O. Ronneberger, R. Nitschke, W. Driever, H. Burkhardt, “Spatially-variant Lucy-Richardson Deconvolution for Multiview Fusion of Microscopical 3D Images”, in IEEE International Symposium on Biomedical Imaging, Chicago, IL, USA, pp. 899-904, 2011.

- [7] J. B. de Monvel, E. Scarfone, S. Le Calvez, M. Ulfendahl, "Image-Adaptative Deconvolution for Three-Dimensional Deep Biological Imaging", *Biophysical Journal*, Vol. 85, pp.3991-4001, 2003.
- [8] M. Faisal, A. D. Lanterman, D. L. Snyder, R. L. White, "Implementation of a Modified Richardson-Lucy Method for Image Restoration on a Massively Parallel Computer to compensate for Space-variant Point Spread of a Charge-coupled-device Camera", *Journal of the Optical Society of America A*, Vol. 12, Issue 12, pp. 2593-2603, 1995.
- [9] H. Cheong, E. Chae, E. Lee, G. Jo, J. Paik, "Fast Image Restoration for Spatially Varying Defocus Blur of Imaging Sensor", *Sensors*, Vol. 15, No.1, pp. 880-898, 2015.
- [10] D. A. Fish, A. M. Brinicombe, E. R. Pike, J. G. Walker, "Blind deconvolution by Means of the Richardson-Lucy algorithm", *J. Opt. Soc. America A*, Vol. 12, No. 1, pp. 58-65, 2005.
- [11] F. Krejci, J. Jakubek, J. Dammer, D. Vavrik, "Enhancement of Spatial Resolution of Roentgenographic Methods", *Nuclear Instruments and Methods in Physics Research A*, Vol. 607, pp. 208-211, 2009.
- [12] F. Aouinti, M. Nasri, M. Moussaoui, "Estimating the Size of the Point Spread Function using Fuzzy Logic for Blind Restoration of Satellite Image", *International Journal of Recent Contributions from Engineering, Science & IT - iJES*, Vol.5, No. 4, pp. 48-59, 2017.
- [13] G. L. Almeida, M. I. Silvani, "A Novel Algorithm for Blind Deconvolution applied to the Improvement of Radiographic Images", in *AIP Conference Proceedings*, Sao Sebastiao, SP, Brazil, Vol. 1529, pp. 95-99, 2013.
- [14] R. L. White, "Image Restoration using the Damped Richardson – Lucy Method", *The Restoration of HST Images and Spectra II Space 01 Telescope Science Institute*, R. J. Hanisch and R. L. White, Eds, 1994.
- [15] B. Masschaele, M. Dierick, L. V. Hoorebeke, P. Jacobs, J. Vlassenbroeck, V. Cnudde, "Neutron CT Enhancement by Iterative de-blurring of Neutron Transmission Images", *Nuclear Instruments and Methods in Physics Research A*, Vol. 542, Issues 1-3, pp. 361-366, 2005.
- [16] M. Bertero, P. Boccacci, "A Simple Method for the Reduction of Boundary Effects in the Richardson-Lucy Approach to Image Deconvolution", *Astronomy and Astrophysics*, Vol. 437, No. pp. 1-6, 2005.